This article has been accepted for publication in a future issue of this journal, but has not been fully edited. Content may change prior to final publication. Citation information: DOI 10.1109/TEC.2018.2866639, IEEE Transactions on Energy Conversion



# On the Impedance Modeling and Equivalence of AC/DC Side Stability Analysis of a Grid-tied Type-IV Wind Turbine System

Chen Zhang, Xu Cai, Marta Molinas, *Member, IEEE,* Atle Rygg

***Abstract*—Impedance modeling of a Type-IV wind turbine is usually associated with model reductions, e.g. the grid-side converter (GSC) is modeled in detail, whereas the machine-side converter (MSC) is simplified as a constant power load (CPL). Meanwhile, the Nyquist-based stability analyses are normally conducted on the ac side, where the evaluation of the stability margin can be difficult due to the presence of multiple eigen-loci. Although some similar analyses regarding the high-voltage dc systems are performed on the dc side, a justification of the consistency between the ac and dc side analysis is lacking. Therefore, this paper aims to address these issues by first developing a detailed impedance model of the Type-IV wind turbine, and then providing a formal proof of the equivalence between the ac and dc side analysis. The detailed Type-IV wind turbine model is verified by the measured frequency responses from simulations, as well as its correctness in Nyquist-based stability analysis. The MSC modeling effects are further discussed, for which a thorough comparison of the CPL-based model and the detailed model with respect to the stability margin is conducted. As a result, the feasibility of the CPL-based model for stability analysis is clarified.**

***Index Terms*—frequency domain analysis, impedance modeling, Nyquist criterion, stability, wind power.**

## I. Introduction

VOLTAGE source converters (VSCs) serve as the main interface for the grid-integration of renewable energy resources such as wind and solar [1], as well as for the interconnection of ac grids by means of high-voltage dc technology (HVDC) [2]. With large amounts of VSCs connected to grid, interactions among converters, and between converters and grid can lead to stability issues, e.g. the inter-harmonic oscillations in the photovoltaic power plants [3], the sub-synchronous oscillations in the permanent magnetic synchronous generator-based (PMSG, i.e. Type-IV) [4] as well as the doubly-fed induction generator-based (DFIG, i.e. Type-III) [5] wind farms. These practical issues are a great impetus for improving the methodologies specific to VSCs-based systems. Among them, the impedance-based method [6] becomes prevailing since the impedances can be derived by either analytical modeling or measurements [7]. Moreover, the well-known Nyquist Criterion (NC) can be applied to the VSC-grid system for stability analysis, or more generally to an interconnected system that can be partitioned into a source and a load equivalence [8].

Regarding the VSC impedance modeling, there are two main methods: the harmonic linearization method in the phase domain [9] and the typical linearization method in *dq* domain [10]. The obtained impedances are the sequence impedance [11] and the *dq* impedance [12] respectively. It is noted that both of them are characterized as two-by-two matrices with the presence of nonzero off-diagonal terms. It thus gives rise to a concern on how to interpret them and what are their consequences on stability. In this regard, recent modeling works, e.g. a complex transfer function based (e.g. [13] and [14]), a modified sequence domain based (e.g. [15] and [16]) and a phasor based method [17], provide some useful insights into the VSC properties. From them, the mirror frequency coupling effect [15] or equivalently the sequence coupling effect [18] are revealed, and it is addressed e.g. in [18] and [19] that these couplings are important for the VSC's stability.

The above-mentioned methods are applicable for wind turbine systems (e.g. [4], [20]-[24]), however, it can be challenging because the wind turbine system is more complex than a single VSC case. Considering this, impedance modeling of a wind turbine system is usually associated with model reductions. For example, in the case of a Type-IV wind turbine, the machine-side converter (MSC) is usually simplified as a constant power load (CPL), whereas the grid-side converter (GSC) is modeled in detail (e.g. [4] and [21]). On the other hand, in the case of a Type-III wind turbine, the dc voltage of the converter is usually assumed constant so that the GSC and RSC are decoupled in the dc side and can be modeled separately (e.g. [23], [24]). Although these model reductions render an easier impedance modeling work, they can lead to inaccuracies when it comes to stability analysis, particularly if the system under discussion is close to its marginal state.

Besides, the generation devices (e.g. the wind turbine) usually conduct their Nyquist-based stability analysis at the ac

"The work and related research are supported by the National Natural Science Foundation of China (51677117), and the Key Laboratory of Control of Power Transmission and Conversion (SJTU), Ministry of Education (2015AC05)".

Chen Zhang is with the Key Laboratory of Control of Power Transmission and Conversion (Shanghai Jiao Tong University), Ministry of Education, Shanghai, 200240, China (Email: nealbc@sjtu.edu.cn).

Xu Cai is with the Department of Electrical Engineering of Shanghai Jiao Tong University, Shanghai, 200240, China (Email: xucai@sjtu.edu.cn).

Marta Molinas and Atle Rygg are with the Department of Engineering Cybernetics, Norwegian University of Science and Technology, Trondheim, 7034, Norway (Email: marta.molinas@ntnu.no; atle.rygg@ntnu.no).

This article has been accepted for publication in a future issue of this journal, but has not been fully edited. Content may change prior to final publication. Citation information: DOI 10.1109/TEC.2018.2866639, IEEE Transactions on Energy Conversion



side. Whereas for the transmission devices (e.g. the VSC-HVDC), it is preferable to perform the stability analysis on the dc side (e.g. [25] and [26]) since the dc side impedances are scalars [25] in contrast to the two-by-two matrices of the ac side. Due to this mismatch in model dimension, though the Nyquist-based analysis can be applied to both sides, their consistency in stability estimates has not been justified.

Therefore, this work aims to address these issues along with a clarification of several significant concerns on the modeling and stability analysis. The rest of paper is organized as follows:

In section II, a modular modeling approach is introduced and applied to derive the detailed impedance model of the Type-IV wind turbine system. Section III provides the proof of the equivalence between the ac and dc side analysis. Section IV discusses the MSC modeling effect on stability analysis. Finally, section V draws the main conclusions. All the analyses are verified by time domain simulations in PSCAD/EMTDC.

## II. Modular Impedance Modeling of a Grid-tied Type-IV Wind Turbine System

### A. Modular modeling method

Fig. 1 (a) shows a typical Type-IV wind turbine system under analysis. The *dq* impedance modeling of a VSC is presented in [12], where a step-by-step linearization of all the control blocks is adopted. This method is inefficient if applied to a system with multiple ac/dc ports as the Type-IV wind turbine. Therefore, on top of [12], this paper adopts a modular modeling approach, where the Type-IV wind turbine system is partitioned into several subsystems, and for each subsystem, it is modeled as a multi-port module, see Fig. 1 (b).

The major benefit of the modular modeling approach is that it renders an efficient way to assemble the ac and dc side impedances without modifying the building blocks of each module, this feature is frequently adopted in this work.

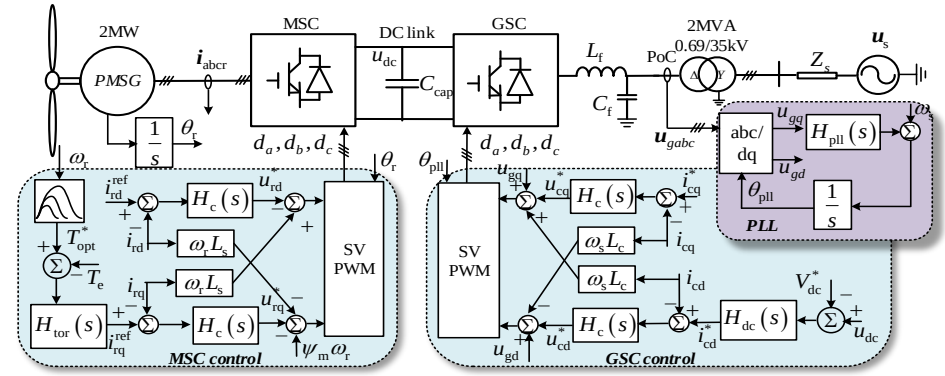


(a) Schematic of a typical grid-tied Type IV wind turbine system

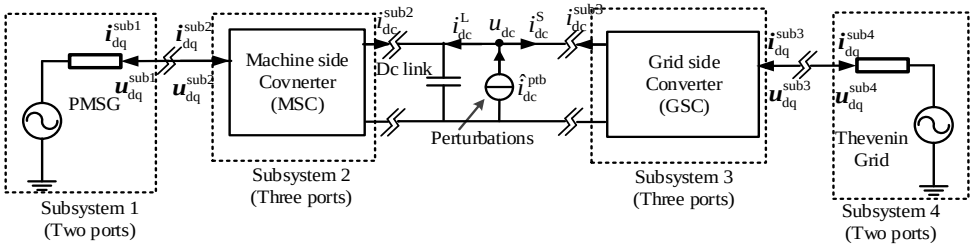


(b) Illustration of the modular modeling approach

Fig. 1. Schematic of the grid-tied Type-IV wind turbine system and the modular modeling approach

Specifically, the PMSG and the ac grid can be modeled as the *two-port* modules in *dq* domain (ac currents flow into the subsystems are positive), e.g.:

$$\begin{bmatrix} u_{\mathrm{d}}^{\mathrm{sub1,4}} \\ u_{\mathrm{q}}^{\mathrm{sub1,4}} \end{bmatrix} = \begin{bmatrix} Z_{\mathrm{dd}}^{\mathrm{sub1,4}}(s) & Z_{\mathrm{dq}}^{\mathrm{sub1,4}}(s) \\ Z_{\mathrm{qd}}^{\mathrm{sub1,4}}(s) & Z_{\mathrm{qq}}^{\mathrm{sub1,4}}(s) \end{bmatrix} \begin{bmatrix} i_{\mathrm{d}}^{\mathrm{sub1,4}} \\ i_{\mathrm{q}}^{\mathrm{sub1,4}} \end{bmatrix} = \boldsymbol{Z}_{\mathrm{dq}}^{\mathrm{sub1,4}}(s) \begin{bmatrix} i_{\mathrm{d}}^{\mathrm{sub1,4}} \\ i_{\mathrm{q}}^{\mathrm{sub1,4}} \end{bmatrix} \tag{1}$$

If the PMSG is considered, the superscripts "1" should be replaced with "PMSG", e.g. $\boldsymbol{Z}_{\mathrm{dq}}^{\mathrm{PMSG}}$. The superscripts "4" are replaced with "Grid" (e.g. $\boldsymbol{Z}_{\mathrm{dq}}^{\mathrm{Grid}}$), if the grid is considered.

$$\begin{bmatrix} i_{\mathrm{d}}^{\mathrm{sub2,3}} \\ i_{\mathrm{q}}^{\mathrm{sub2,3}} \\ i_{\mathrm{dc}}^{\mathrm{sub2,3}} \end{bmatrix} = \begin{bmatrix} \boldsymbol{Y}_{\mathrm{dq}}^{\mathrm{sub2,3}}(s) & \boldsymbol{a}_{2\times1}^{\mathrm{sub2,3}}(s) \\ \boldsymbol{b}_{1\times2}^{\mathrm{sub2,3}}(s) & Y_{\mathrm{dc}}^{\mathrm{sub2,3}}(s) \end{bmatrix} \begin{bmatrix} u_{\mathrm{d}}^{\mathrm{sub2,3}} \\ u_{\mathrm{q}}^{\mathrm{sub2,3}} \\ u_{\mathrm{dc}}^{\mathrm{sub2,3}} \end{bmatrix} \tag{2}$$

On the other hand, the GSC and MSC can be generally modeled as the *three-port* modules as (2) (ac currents flow into the converters are positive, dc currents flow into the dc-link are positive).

If the MSC is considered, the superscripts "2" should be replaced with "MSC", e.g. $\boldsymbol{Y}_{\mathrm{dq}}^{\mathrm{MSC}}$. The superscripts "3" are replaced with "GSC", e.g. $\boldsymbol{Y}_{\mathrm{dq}}^{\mathrm{GSC}}$, if the GSC is concerned. Transfer-functions of these modules are given in the appendix.

### B. Derivation of the detailed dc side impedance models

Benefit from this modular representation, both the ac and dc side impedance can be assembled efficiently. For example, if the ac side impedance is to be developed, the dc and ac nodes of the MSC and PMSG module should be eliminated by applying basic circuit laws, only the ac nodes of the GSC are retained. This paper will focus on the dc side impedance modeling and analysis, whereas the ac side impedance model will be briefly provided along with the proof in section III.

This article has been accepted for publication in a future issue of this journal, but has not been fully edited. Content may change prior to final publication. Citation information: DOI 10.1109/TEC.2018.2866639, IEEE Transactions on Energy Conversion



The dc side impedances can be developed by eliminating all the ac nodes, e.g. the interface of PMSG and MSC. According to the Fig. 1 (b), this can be fulfilled by further finding the following equations in addition to (1) and (2):

$$\begin{bmatrix} i_{\mathrm{d}}^{\mathrm{PMSG}} \\ i_{\mathrm{q}}^{\mathrm{PMSG}} \end{bmatrix} + \begin{bmatrix} i_{\mathrm{d}}^{\mathrm{MSC}} \\ i_{\mathrm{q}}^{\mathrm{MSC}} \end{bmatrix} = 0, \begin{bmatrix} i_{\mathrm{d}}^{\mathrm{GSC}} \\ i_{\mathrm{q}}^{\mathrm{GSC}} \end{bmatrix} + \begin{bmatrix} i_{\mathrm{d}}^{\mathrm{Grid}} \\ i_{\mathrm{q}}^{\mathrm{Grid}} \end{bmatrix} = 0 \tag{3}$$

$$\begin{bmatrix} u_{\mathrm{d}}^{\mathrm{PMSG}} \\ u_{\mathrm{q}}^{\mathrm{PMSG}} \end{bmatrix} = \begin{bmatrix} u_{\mathrm{d}}^{\mathrm{MSC}} \\ u_{\mathrm{q}}^{\mathrm{MSC}} \end{bmatrix}, \begin{bmatrix} u_{\mathrm{d}}^{\mathrm{GSC}} \\ u_{\mathrm{q}}^{\mathrm{GSC}} \end{bmatrix} = \begin{bmatrix} u_{\mathrm{d}}^{\mathrm{Grid}} \\ u_{\mathrm{q}}^{\mathrm{Grid}} \end{bmatrix} \tag{4}$$

Since (1)-(4) have 18 independent equations and 20 unknown variables, two sets of linear dependent variables can be found, e.g. $u_{\mathrm{dc}}^{\mathrm{MSC}} \leftrightarrow i_{\mathrm{dc}}^{\mathrm{MSC}}$ and $u_{\mathrm{dc}}^{\mathrm{GSC}} \leftrightarrow i_{\mathrm{dc}}^{\mathrm{GSC}}$. This linear dependence can be interpreted as the dc side impedance or dc side admittance:

$$\begin{aligned} & i_{\mathrm{dc}}^{\mathrm{MSC}} = Y_{\mathrm{dc}}^{1,2}(s) \cdot u_{\mathrm{dc}}^{\mathrm{MSC}} \rightarrow \\ & Y_{\mathrm{dc}}^{1,2}(s) = \boldsymbol{b}_{1\times 2}^{\mathrm{MSC}} \cdot \left( \boldsymbol{Y}_{\mathrm{dq}}^{\mathrm{PMSG}} + \boldsymbol{Y}_{\mathrm{dq}}^{\mathrm{MSC}} \right)^{-1} \boldsymbol{a}_{2\times 1}^{\mathrm{MSC}} - Y_{\mathrm{dc}}^{\mathrm{MSC}} \end{aligned} \tag{5}$$

$$\begin{aligned} & u_{\mathrm{dc}}^{\mathrm{GSC}} = Z_{\mathrm{dc}}^{3,4}(s) \cdot i_{\mathrm{dc}}^{\mathrm{GSC}} \rightarrow \\ & Z_{\mathrm{dc}}^{3,4}(s) = 1 / \left[ \boldsymbol{b}_{1\times 2}^{\mathrm{GSC}} \cdot \left( \boldsymbol{Y}_{\mathrm{dq}}^{\mathrm{Grid}} + \boldsymbol{Y}_{\mathrm{dq}}^{\mathrm{GSC}} \right)^{-1} \boldsymbol{a}_{2\times 1}^{\mathrm{GSC}} - Y_{\mathrm{dc}}^{\mathrm{GSC}} \right] \end{aligned} \tag{6}$$

According to Fig. 1 (b), the dc side equivalent circuit is drawn in Fig. 2. It presents a typical source-load type system that is suitable for Nyquist-based stability analysis [6]. In which, the source impedance is defined as: $Z_{\mathrm{dc}}^{\mathrm{S}}(s) = Z_{\mathrm{dc}}^{3,4}(s)$, and the load admittance is defined as: $Y_{\mathrm{dc}}^{\mathrm{L}}(s) = Y_{\mathrm{dc}}^{1,2}(s) + sC_{\mathrm{cap}}$.

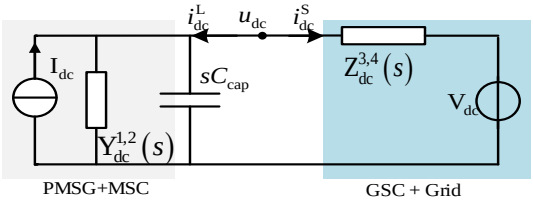


Fig. 2. The dc side equivalent circuit of the Type-IV wind turbine system

## C. *Model verification by the measured frequency responses*

In this section, the developed analytical models (i.e. $Z_{\mathrm{dc}}^{\mathrm{S}}$ and $Y_{\mathrm{dc}}^{\mathrm{L}}$) will be compared with the measured frequency responses from time domain simulations. The simulation model is shown in Fig. 1 (a). And the main parameters are listed in Table I.

Table I Main parameters

| PMSG | | VSC | |
|---|---|---|---|
| Name | Value | Name | Value |
| Frequency $f_{\mathrm{rn}}$ | 15 Hz | Power rating $S_{\mathrm{b}}$ | 2 MVA |
| Voltage $V_{\mathrm{n}}$ | 690 V | Rate voltage $V_{\mathrm{n}}$ | 690 V |
| Pole pairs $p$ | 45 | dc voltage $V_{\mathrm{dc}}$ | 1.1 kV |
| Magnetic flux $\varphi_{\mathrm{m}}$ | 7.57 Wb | dc capacitance $C_{\mathrm{cap}}$ | 30 mF |
| Stator resistance $R_{\mathrm{s}}$ | 0.001 ohm | Switching frequency $f_{\mathrm{s}}$ | 1.4kHz |
| Stator reactance $L_{\mathrm{s}}$ | 1.1 mH | Filter inductance $L_{\mathrm{f}}$ | 0.076 mH |

A shunt current harmonic source as depicted in Fig. 1 (b) is applied to inject small signal perturbations. The multi-run module in PSCAD is utilized to fulfill the single-tone injection for each run. The perturbation frequency is varying from 1 to 100 Hz with an increment of 1 Hz. Then, the simulation data e.g. $i_{\mathrm{dc}}^{\mathrm{L}}(t), i_{\mathrm{dc}}^{S}(t), u_{\mathrm{dc}}(t)$ (the sampling rate is 1 kHz and the time frame is 1 s) are collected and sent to MATLAB for the data process. Finally, the measured frequency responses are plotted together with the analytical models as shown in the following.

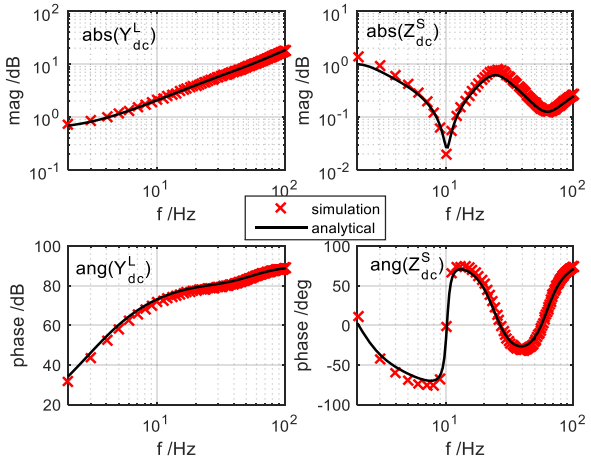


(a) PMSG angular speed $\omega_{\mathrm{r0}}$ = 0.7 pu, torque $T_{\mathrm{e0}}$ = 0.5 pu, i.e. $P_0$ = 0.35 p.u.

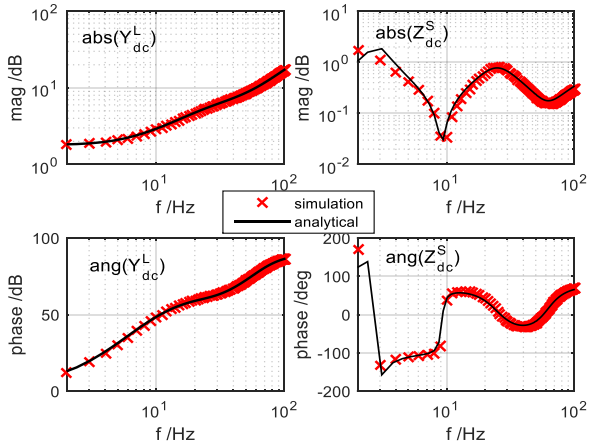


(b) PMSG angular speed $\omega_{\mathrm{r0}}$ = 1 pu, torque $T_{\mathrm{e0}}$ = 1 pu, i.e. $P_0$ = 1 p.u

Fig. 3. Comparison of the analytical models and the measured frequency responses (torque and dc voltage control bandwidth (BD) are 20 Hz, MSC/GSC current control BD are 200 Hz, PLL = 20 Hz, SCR = 4)

In Fig. 3, both a light load (i.e. $P_0$= 0.35 pu) and a heavy load condition (i.e. $P_0$= 1 pu) are taken into account. In general, both the source ($Z_{\mathrm{dc}}^{\mathrm{S}}$) and the load ($Y_{\mathrm{dc}}^{\mathrm{L}}$) model are matched with the measured frequency responses from the simulations, indicating that the developed impedance models are effective for relevant stability analysis within the frequency range of interest (in this work the concerned frequency range is below 100 Hz, and the frequency is measured in the *dq* frame).

It can also be observed that the source impedance ($Z_{\mathrm{dc}}^{\mathrm{S}}$) exhibits multiple changes in phase characteristics (e.g. from capacitive to inductive), implying the existence of resonances in $Z_{\mathrm{dc}}^{\mathrm{S}}$. In this case, these resonances are stable since the frequency responses can only be measured under a stable system. In other cases, they can be unstable, however, the final stability conclusion can only be determined by further including the effects of the load admittance, i.e. the closed-loop stability. This will be discussed in section IV.

This article has been accepted for publication in a future issue of this journal, but has not been fully edited. Content may change prior to final publication. Citation information: DOI 10.1109/TEC.2018.2866639, IEEE Transactions on Energy Conversion



## III. Proof and Analysis of the Identical AC and DC Side Marginal Stability Condition

As mentioned before, there are several advantages to conduct analysis on the dc side, e.g. the dc side impedances are scalars, making the interpretation, measurement as well as the stability analysis easier. In contrast, the ac side impedances are matrices, thus the physical interpretation can be difficult, and also the Generalized Nyquist Criterion (GNC) [27] has to be applied for stability analysis.

Technically, although the Nyquist Criterion can apply to both sides, the model dimension involved in the calculation is different and a straightforward equivalence is not evident. To verify there is no critical information loss due to this dimension mismatch, a proof of the equivalence is necessary.

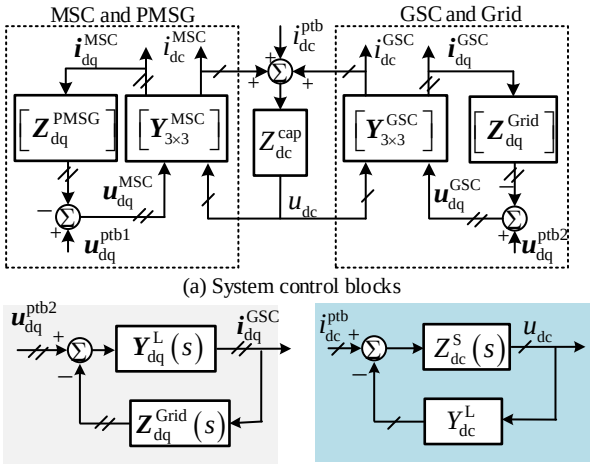


Fig. 4. Control blocks diagrams of the grid-tied Type IV system

First, in accordance with the Fig. 1 (b), the control block diagram can be drawn in Fig. 4 (a), in which e.g. $i_{dc}^{ptb}$ and $\boldsymbol{u}_{dq}^{ptb}$ represent the independent perturbations of the dc and the ac side respectively.

Then, if the stability analysis is conducted on the ac side, i.e. $\boldsymbol{u}_{dq}^{ptb2}$ will take effects, the closed-loop system of the ac side can be drawn in Fig. 4 (b). Likewise, the closed-loop system of the dc side can be drawn in Fig. 4 (c).

In the next, the *marginal stability condition* of the ac and dc side analysis will be developed and compared.

### A. Marginal stability condition of the dc side analysis

Since the control blocks of the dc side analysis as shown in Fig. 4 (c) have already been developed, i.e. (5) and (6), the minor loop gain can be directly derived as: $L_{DC}(s)=Z_{dc}^{S}\cdot Y_{dc}^{L}(s)$.

Then, according to the Nyquist criterion, the marginal stability condition can be described as:

$$\det\left[\lambda - L_{DC}(s)\right]=0 \text{ if } \lambda=-1 \tag{7}$$

Rewriting (7) by substituting $L_{DC}(s)$ yields the dc side *marginal stability condition* as:

$$Y_{dc}^{L}-Y_{dc}^{GSC}+\boldsymbol{b}_{1\times2}^{GSC}\cdot\left(\boldsymbol{Y}_{dq}^{Grid}+\boldsymbol{Y}_{dq}^{GSC}\right)^{-1}\boldsymbol{a}_{2\times1}^{GSC}=0 \tag{8}$$

### B. Marginal stability condition of the ac side analysis

First, the ac side impedance models should be developed. This can be fulfilled by finding the following equations in addition to (1) and (2):

$$\begin{bmatrix} i_d^{PMSG} \\ i_q^{PMSG} \end{bmatrix}+\begin{bmatrix} i_d^{MSC} \\ i_q^{MSC} \end{bmatrix}=0,\begin{bmatrix} u_d^{PMSG} \\ u_q^{PMSG} \end{bmatrix}=\begin{bmatrix} u_d^{MSC} \\ u_q^{MSC} \end{bmatrix} \tag{9}$$

$$\begin{aligned} i_{dc}^{MSC}+i_{dc}^{GSC}&=sC_{cap}u_{dc} \\ u_{dc}^{MSC}=u_{dc},&u_{dc}^{GSC}=u_{dc} \end{aligned} \tag{10}$$

and eliminating the dc/ac nodes of the MSC/PMSG modules.

Since there are 21 unknown and 17 independent equations, four sets of linear-dependent variables can be found, e.g. $\boldsymbol{u}_{dq}^{GSC}\leftrightarrow\boldsymbol{i}_{dq}^{GSC}$ and $\boldsymbol{u}_{dq}^{Grid}\leftrightarrow\boldsymbol{i}_{dq}^{Grid}$. As a result, the grid impedance and the ac side GSC admittance (i.e. $\boldsymbol{Y}_{dq}^{L}$, including the MSC, PMSG and dc capacitor) in Fig. 4 (b) can be derived:

$$\begin{aligned} \boldsymbol{u}_{dq}^{Grid}&=\boldsymbol{Z}_{dq}^{Grid}\cdot\boldsymbol{i}_{dq}^{Grid} \\ \boldsymbol{i}_{dq}^{GSC}&=\boldsymbol{Y}_{dq}^{L}\cdot\boldsymbol{u}_{dq}^{GSC}\rightarrow \\ \boldsymbol{Y}_{dq}^{L}&=\boldsymbol{Y}_{dq}^{GSC}+\boldsymbol{a}_{2\times1}^{GSC}\left(Y_{dc}^{L}-Y_{dc}^{GSC}\right)^{-1}\boldsymbol{b}_{1\times2}^{GSC} \end{aligned} \tag{11}$$

Based on (11), the ac side minor loop gain is obtained as: $\boldsymbol{L}_{AC}(s)=\boldsymbol{Z}_{dq}^{Grid}\cdot\boldsymbol{Y}_{dq}^{L}(s)$. Then according to the GNC, the marginal stability condition is described as:

$$\det\left[\lambda\boldsymbol{I}_{2\times2}-\boldsymbol{L}_{AC}(s)\right]=0 \text{ if } \lambda=-1 \tag{12}$$

Rewriting (12) by substituting $\boldsymbol{L}_{AC}(s)$ yields the ac side *marginal stability condition* as:

$$\det\left[\left(Y_{dc}^{L}-Y_{dc}^{GSC}\right)\boldsymbol{I}_{2\times2}+\left(\boldsymbol{Y}_{dq}^{Grid}+\boldsymbol{Y}_{dq}^{GSC}\right)^{-1}\boldsymbol{a}_{2\times1}^{GSC}\cdot\boldsymbol{b}_{1\times2}^{GSC}\right]=0 \tag{13}$$

### C. Check for the equivalence

The ac/dc side marginal stability condition as developed in (8) and (13) are implicit, to render an explicit comparison, the notation:

$$\boldsymbol{N}=\boldsymbol{M}\cdot\boldsymbol{a}_{2\times1}^{GSC}\cdot\boldsymbol{b}_{1\times2}^{GSC}=\begin{bmatrix} n_{11} & n_{12} \\ n_{21} & n_{22} \end{bmatrix} \tag{14}$$

is defined, where

$$\boldsymbol{M}=\left(\boldsymbol{Y}_{dq}^{Grid}+\boldsymbol{Y}_{dq}^{GSC}\right)^{-1}=\begin{bmatrix} m_{11} & m_{12} \\ m_{21} & m_{22} \end{bmatrix} \tag{15}$$

Then, the ac side marginal stability condition (13) can be rewritten as:

$$\begin{aligned} &\det\left(\lambda\cdot\boldsymbol{I}_{2\times2}+\boldsymbol{N}\right)=0\rightarrow \\ &\lambda^2+\left(n_{11}+n_{22}\right)\lambda+n_{11}n_{22}-n_{12}n_{21}=0 \end{aligned} \tag{16}$$

where $n_{11}n_{22}-n_{12}n_{21}=\det\boldsymbol{N}=\det\boldsymbol{M}\cdot\det\left(\boldsymbol{a}_{2\times1}^{GSC}\cdot\boldsymbol{b}_{1\times2}^{GSC}\right)$.

Examining the determinant of $\boldsymbol{a}_{2\times1}^{GSC}\cdot\boldsymbol{b}_{1\times2}^{GSC}$ yields that: $\det\left(\boldsymbol{a}_{2\times1}^{GSC}\cdot\boldsymbol{b}_{1\times2}^{GSC}\right)=0$ for any vectors $\boldsymbol{a}_{2\times1}^{GSC}$ and $\boldsymbol{b}_{1\times2}^{GSC}$. As a result, $\det\boldsymbol{N}=0$ is obtained. As a result, the eigenvalues of (16) are derived as: $\lambda_1=0,\lambda_2=-\left(n_{11}+n_{22}\right)$.

This article has been accepted for publication in a future issue of this journal, but has not been fully edited. Content may change prior to final publication. Citation information: DOI 10.1109/TEC.2018.2866639, IEEE Transactions on Energy Conversion



By exploring (13) it can be identified that $Y_{dc}^{L}-Y_{dc}^{GSC}$ is actually the nonzero eigenvalue of (16), therefore

$$Y_{dc}^{L}-Y_{dc}^{GSC}=\lambda_2=-\left(n_{11}+n_{22}\right)$$
$$=a_1^{GSC}b_1^{GSC}m_{11}+a_2^{GSC}b_1^{GSC}m_{12}+a_1^{GSC}b_2^{GSC}m_{21}+a_2^{GSC}b_2^{GSC}m_{22} \quad (17)$$

where $\boldsymbol{a}_{2\times1}^{GSC}=\begin{bmatrix}a_1^{GSC} & a_2^{GSC}\end{bmatrix}^T$, and $\boldsymbol{b}_{1\times2}^{GSC}=\begin{bmatrix}b_1^{GSC} & b_2^{GSC}\end{bmatrix}$.

Similarly, by substituting $\boldsymbol{M}$ into (8) yields the dc side marginal stability condition in the explicit format is:

$$Y_{dc}^{L}-Y_{dc}^{GSC}=b_1^{GSC}\left(a_1^{GSC}m_{11}+a_2^{GSC}m_{21}\right)+ b_2^{GSC}\left(a_1^{GSC}m_{12}+a_2^{GSC}m_{22}\right) \quad (18)$$

Comparing (17) and (18) it can be found that, the dc and ac side analysis are equivalent in terms of the marginal stability.

A further comment should be made on the model dimensions. In this proof, the equivalence of ac and dc side analysis is achieved because both the ac and the dc side impedance models can be accurately modeled, which means they have finite dimensions. This is correct as long as the three-phase system is symmetric. However, if an asymmetric grid is concerned, an accurate modeling of the system can be difficult due to the time-varying property. This feature, in the frequency domain, can be captured by the harmonic transfer function [28], which are generally doubly-infinite dimensional matrices that cannot be directly used for analysis. Therefore, matrix truncations are necessary, and this in return, may lead to inconsistency between ac and dc side analysis.

### *D. Verification of the proof by Nyquist-based analysis*

In the following, the identical ac and dc side marginal stability condition will be verified by comparing their Nyquist plots and checking whether they approach the critical point simultaneously.

In the first place, a stable case is compared in Fig. 5 (a). It can be seen that both the dc and ac side Nyquist plots predict a stable system since there are no encirclements of the critical point (-1, 0 j).

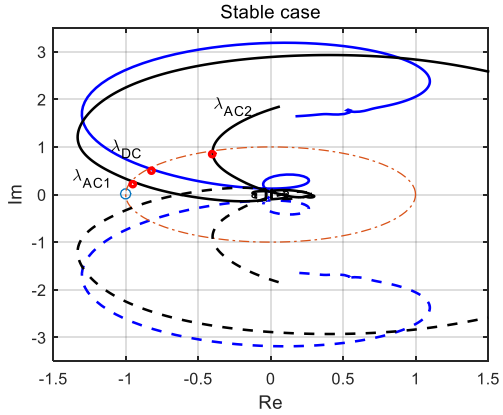


(a) A stable case (PLL = 20 Hz, black color: the ac side Nyquist plots, blue color: the dc side Nyquist plots)

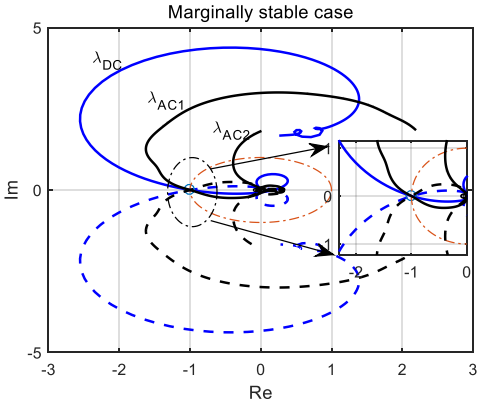


(b) A marginally stable case (PLL = 45 Hz, black color: the ac side Nyquist plots, blue color: the dc side Nyquist plots)

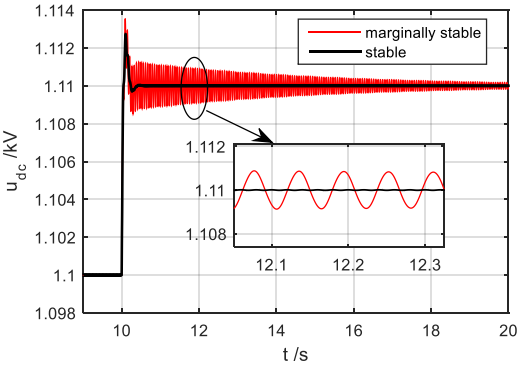


(c) Time response of the dc voltage (at 10s, the dc voltage set-point is increased by a small value, i.e. 0.01 kV)

Fig. 5 Nyquist plots of the ac and dc side (dc voltage control BD is 40 HZ, MSC/GSC current control BD are 200 Hz, torque control BD is 20 Hz, SCR = 4, $P_0$= 0.35 pu)

However, due to the Nyquist plots of the ac side present two eigenvalue loci, it is difficult to determine and evaluate the stability margin. For example, in Fig. 5 (a), $\lambda_{AC1}$ is close to the critical point indicating a small phase margin, whereas $\lambda_{AC2}$ indicates a relatively large phase margin. However, the total margin cannot be determined in an intuitive way. In contrast, the dc side analysis can provide more straightforward margin information due to only one eigenvalue locus is presented. For example, the phase margin from the dc side analysis can be evaluated at the intersection point between $\lambda_{DC}$ and the unit circle in Fig. 5 (a).

Then, a marginally stable condition is established by increasing the PLL bandwidth as shown in Fig. 5 (b). As can be seen, both the ac and dc side eigenvalue loci approximately arrived at the critical point with the same pace. This observation justifies the former proof.

In order to verify the Nyquist-based analysis, time domain simulations are conducted and presented in Fig. 5 (c), in which a small step change in the dc voltage reference is applied. It can be seen that the dc voltage response of the stable case is well damped since the relatively large phase margin as indicated from the dc side Nyquist plots of the Fig. 5 (a). On the other hand, the dc voltage response under the marginally stable case is poorly damped, proving that the Nyquist-based analysis is correct.

This article has been accepted for publication in a future issue of this journal, but has not been fully edited. Content may change prior to final publication. Citation information: DOI 10.1109/TEC.2018.2866639, IEEE Transactions on Energy Conversion



## IV. The MSC Modeling Effects on the Stability Analysis

This section will further discuss the MSC modeling effects on the stability analysis of the Type-IV wind turbine, for which a commonly used CPL-based model (e.g. [12]) will be compared with the detailed MSC model in terms of stability margin. This analysis will be performed on the dc side since it will not lose the generality in stability conclusion but can provide more intuitive margin information as discussed earlier.

### *A. A qualitative study of the MSC modeling effects*

The detailed MSC model is developed in (5), i.e. $Y_{\mathrm{dc}}^{1,2}$, whereas the CPL model is straightforward, i.e. $Y_{\mathrm{dc}}^{1,2} \approx P_0 / V_{\mathrm{dc0}}^2$.

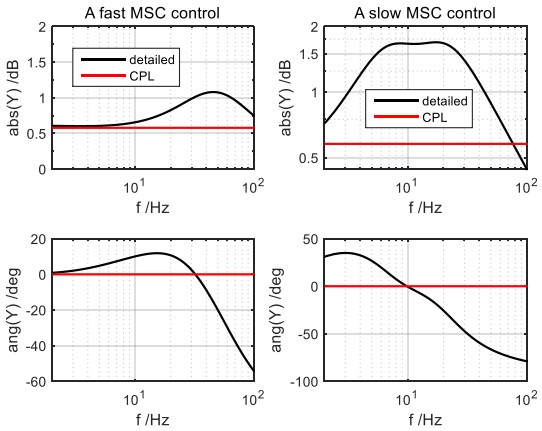


(a) Bode plots of the CPL and the detailed MSC model (Fast: MSC current control BD = 200 Hz. Slow: MSC current control BD = 50 Hz. Torque control BD is a decade smaller than the current control. $P_0$ = 0.35 pu)

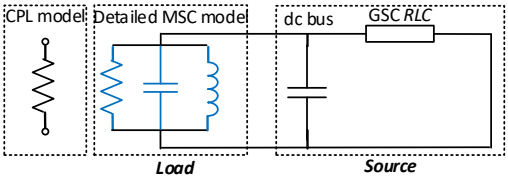


(b) A physical interpretation of the MSC modeling effects

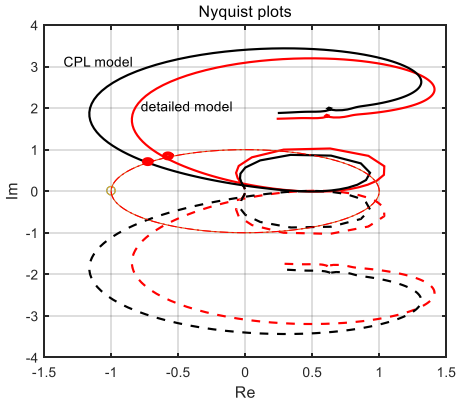


(c) Nyquist-based analysis of the MSC modeling effects (MSC current control = 100 Hz, GSC current control = 200 Hz, dc voltage control = 20 Hz, PLL = 20 Hz. $P_0$ = 0.35 pu)

Fig. 6 A qualitatively study of the MSC modeling effects on stability

Bode plots of the CPL and the detailed MSC model are first compared in Fig. 6 (a). It can be observed that the CPL model does not match with the detailed model in general, particularly under a slow MSC control configuration.

Specifically, at the low-frequency range, the detailed MSC model exhibits some capacitive characteristics, whereas for the high-frequency range, it presents inductive characteristics. This finding in combination with the characteristics of the source impedance in Fig. 3, allowing us to qualitatively draw the circuit model as in Fig. 6 (b). From this, the MSC modeling effects can be physically interpreted as follows: the CPL model only has resistive effects on the source impedance, whereas the detailed MSC can further shape the modes (i.e. the resonances of the source impedance) by its internal *LC* circuit.

It should be noted that this additional freedom of the detailed MSC model can affect the closed-loop stability a lot. For example, suppose the source impedance has a pair of unstable mode, which can be qualitatively described as: $Z_{\mathrm{source}} = \dfrac{1}{s^2 + as + b}$ with the conditions: $a < 0$ and $b > 0$. Then the closed-loop system is: $G_{cl}(s) = \dfrac{Z_{\mathrm{source}}(s)}{1 + Z_{\mathrm{source}}(s) Y_{\mathrm{load}}(s)}$.

For the CPL model: $Y_{\mathrm{load}} = G$, thus the closed-loop system is: $G_{cl}(s) = \dfrac{1}{s^2 + as + b + G}$. It can be identified that the CPL model does not change the property of the closed-loop stability.

However, for the detailed MSC model, if the capacitive characteristic is concerned, then its model can be qualitatively written as: $Y_{\mathrm{load}} = G + sC$, thus $G_{cl}(s) = \dfrac{G + sC}{s^2 + (a + C)s + b + G}$ is obtained. Clearly, if $a + C > 0$, the system can be stabilized.

Given by this qualitative analysis, it seems that the CPL model can be pessimistic for stability analysis. To verify this, the dc side Nyquist plots of the CPL-based and the detailed model are compared in Fig. 6 (c). From the intersection points, it is obtained that the CPL model predicts less phase margin than the detailed model.

In order to check whether this pessimism of the CPL model holds for a wide range, in the following, stability margin will be evaluated under various system configurations.

### *B. Stability margin analysis*

In this section, the focus is placed on the phase margin since it is tightly related to the damping of a dynamical system. It can be numerically calculated as, $\varphi_m = 180 - \angle L_{\mathrm{DC}}(\mathrm{j}\omega_c)$ when $|L_{\mathrm{DC}}(\mathrm{j}\omega_c)| = 1$. Based on this method, the phase margins of the CPL-based and the detailed model under various configurations are compared in Fig. 7 (a)-(c). Since the effects of the MSC are most concerned, all the curves are plotted against the MSC current control bandwidth.

From an overview of Fig. 7 (a)-(c) it can be identified that the CPL model, in general, predicts less phase margin than the detailed model. In detail, the differences between the CPL and the detailed model are more evident under a small MSC control BD than a large one. This implies that the CPL model can be a good approximation if the MSC control is fast. However, a fast MSC control is not beneficial for the overall stability.

This article has been accepted for publication in a future issue of this journal, but has not been fully edited. Content may change prior to final publication. Citation information: DOI 10.1109/TEC.2018.2866639, IEEE Transactions on Energy Conversion



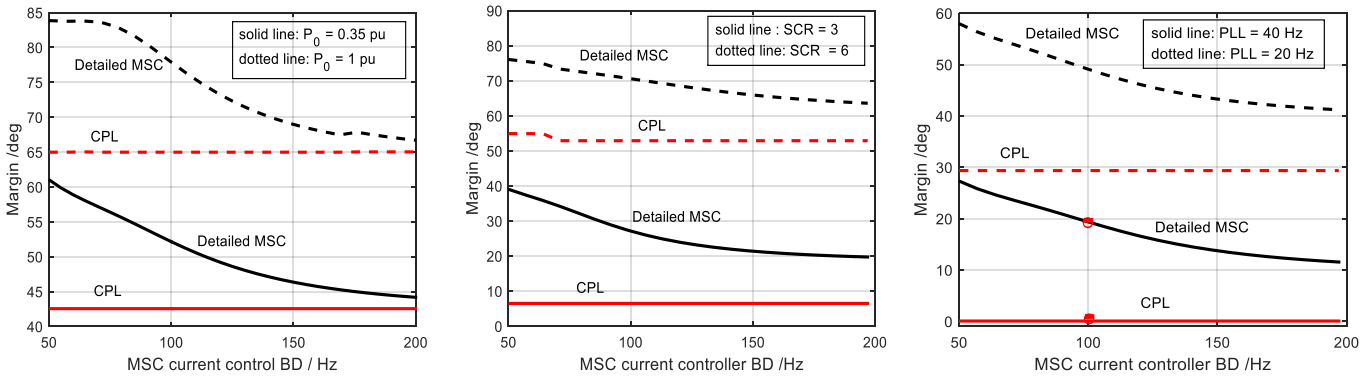


(a) Effects of operating point (SCR = 4, PLL = 20 Hz) (b) Effects of SCR (PLL = 20 Hz, $P_0$ = 0.35 pu) (c) Effects of PLL (SCR = 4, $P_0$ = 0.35 pu)

Fig. 7 Phase margin comparisons (GSC current and dc voltage control BD are 200 Hz and 40 Hz. MSC torque control BD is a decade smaller than the current control BD)

Then, the effects of active power (i.e. the operating point) on the phase margin are depicted in Fig. 7 (a). It shows that, as the output power increases, the overall stability margin is improved. This can be qualitatively explained by the CPL model: $Y_{\mathrm{dc}}^{1,2} \approx P_0 / V_{\mathrm{dc0}}^2$ , where a large output power implies more damping, i.e. more margin.

Next, Fig. 7 (b) presents the effects of the grid SCR on phase margin, it further confirms the knowledge that a weak grid (i.e. a small SCR) can downgrade the overall stability.

Last, the effects of the PLL bandwidth on phase margin are further shown in Fig. 7 (c), from which it can be identified that a slow PLL is beneficial for small signal stability.

### C. A Case study

By exploring the Fig. 7 (c) further it can be obtained that, the CPL-based model predicts a marginally stable system at 100 Hz (marked by a red dot), whereas the detailed model indicates a stable one, moreover, with a decent phase margin.

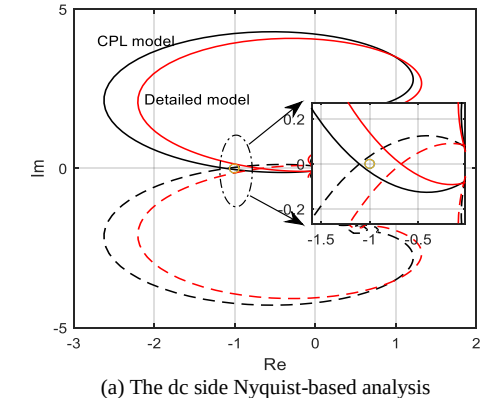


(a) The dc side Nyquist-based analysis

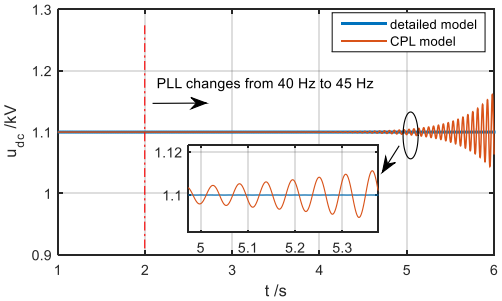


(b) Time domain response of the dc voltage

Fig. 8 A case study of the wrong stability prediction of the CPL model even for a system with a decent stability margin

Under this condition, if the system's margin is further downgraded a little (e.g. by increasing the PLL bandwidth from 40 Hz to 45 Hz), the CPL model will predict a marginally *unstable* system as shown in Fig. 8 (a). However, in fact, the system should be *stable* as indicated by the detailed model.

The corresponding time-domain simulation is presented in Fig. 8 (b), where it can be seen that the detailed model is stable after a small change of the PLL bandwidth. Whereas the CPL model becomes oscillating after a relatively long time since the change of PLL bandwidth, indicating a marginally unstable system. These observations justify the Nyquist-based analysis.

## V. Conclusions

This work provides a detailed impedance model of the Type-IV wind turbine system, along with a clarification of several significant concerns on the modeling and stability analysis:

1) The ac and dc side analysis are equivalent in terms of marginal stability condition, while the equivalence of the stability margin remains an open question.

2) Model reduction of the MSC as a CPL model is too pessimistic for stability analysis. It may lead to wrong stability conclusion even for a system with a decent margin. It points out the need for careful studies on the model reductions of complex systems, particularly for the purposes of stability analysis.

3) A fast MSC control has negative impacts on the stability of a Type-IV wind turbine. This means by slowing down the MSC control, the overall stability margin can be improved. It is feasible for practical implementation because the maximum power tracking of the MSC does not necessarily require a very fast control due to the large inertia of the rotating mass.

## Appendix

### A. Impedance modeling of the PMSG module

The PMSG impedance model is intuitive, which is:

$$\boldsymbol{Z}_{\mathrm{dq}}^{\mathrm{PMSG}} = \begin{bmatrix} R_{\mathrm{s}} + sL_{\mathrm{s}} & -\omega_{\mathrm{r0}} L_{\mathrm{s}} \\ \omega_{\mathrm{r0}} L_{\mathrm{s}} & R_{\mathrm{s}} + sL_{\mathrm{s}} \end{bmatrix} \tag{A.1}$$

where the $R_{\mathrm{s}}$ and $L_{\mathrm{s}}$ are stator resistance and inductance respectively. And, $\boldsymbol{Y}_{\mathrm{dq}}^{\mathrm{PMSG}} = \left(\boldsymbol{Z}_{\mathrm{dq}}^{\mathrm{PMSG}}\right)^{-1}$.

This article has been accepted for publication in a future issue of this journal, but has not been fully edited. Content may change prior to final publication. Citation information: DOI 10.1109/TEC.2018.2866639, IEEE Transactions on Energy Conversion



### B. Impedance modeling of the MSC module

*dq* impedance modeling of a VSC has been extensively discussed in e.g. [12]. In addition to the *dq* ports, the dc port is retained in this work, by linearizing MSC control blocks, the following equation can be obtained:

$$\begin{aligned}\begin{bmatrix} i_{\mathrm{d}}^{\mathrm{MSC}} \\ i_{q}^{\mathrm{MSC}} \end{bmatrix} &= \frac{\boldsymbol{B}^{-1}}{V_{dc0}}\begin{bmatrix} u_{\mathrm{d}}^{\mathrm{MSC}} \\ u_{\mathrm{q}}^{\mathrm{MSC}} \end{bmatrix} - \frac{\boldsymbol{B}^{-1}}{V_{\mathrm{dc0}}}\begin{bmatrix} M_{\mathrm{d0}}^{\mathrm{MSC}} \\ M_{\mathrm{q0}}^{\mathrm{MSC}} \end{bmatrix} u_{dc} \\ &= \boldsymbol{Y}_{\mathrm{dq}}^{\mathrm{MSC}}\begin{bmatrix} u_{\mathrm{d}}^{\mathrm{MSC}} \\ u_{\mathrm{q}}^{\mathrm{MSC}} \end{bmatrix} + \boldsymbol{a}_{2\times1}^{\mathrm{MSC}} \cdot u_{dc}\end{aligned} \tag{A.2}$$

where $\boldsymbol{B} = diag\left\{ \mathrm{H_c} \quad \mathrm{H_c}\left(\frac{3}{2}\psi_{\mathrm{m}} n_{\mathrm{p}} \mathrm{H_{tor}}(s)+1\right)\right\}$, $\psi_{\mathrm{m}}$ is the magnetic flux of PMSG, $n_{\mathrm{p}}$ is the pole pairs. $\mathrm{H_c}(s)$ and $\mathrm{H_{tor}}(s)$ are the current and torque PI controller of MSC.

Further, according to the principle of power balance between ac and dc side, the following equation can be obtained:

$$i_{\mathrm{dc}}^{\mathrm{MSC}} = \boldsymbol{b}_{1\times2}^{\mathrm{MSC}}\begin{bmatrix} u_{\mathrm{d}}^{\mathrm{MSC}} \\ u_{\mathrm{q}}^{\mathrm{MSC}} \end{bmatrix} + Y_{\mathrm{dc}}^{\mathrm{MSC}} \cdot u_{dc} \tag{A.3}$$

where:

$\boldsymbol{b}_{1\times2}^{\mathrm{MSC}} = \frac{3}{2}\left[ M_{\mathrm{d0}}^{\mathrm{MSC}} + I_{\mathrm{d0}}^{\mathrm{MSC}}\mathrm{H_c} \quad M_{\mathrm{q0}}^{\mathrm{MSC}} + I_{\mathrm{q0}}^{\mathrm{MSC}}\mathrm{H_c}\left(\frac{3}{2}\psi_{\mathrm{m}} n_{\mathrm{p}} \mathrm{H_{tor}}(s)+1\right)\right]\frac{\boldsymbol{B}^{-1}}{V_{\mathrm{dc0}}}$; $M_{\mathrm{d0}}^{\mathrm{MSC}}$ and $M_{\mathrm{q0}}^{\mathrm{MSC}}$ are the steady *dq* modulations. $Y_{\mathrm{dc}}^{\mathrm{MSC}} = -\boldsymbol{b}_{1\times2}^{\mathrm{MSC}}\begin{bmatrix} M_{\mathrm{d0}}^{\mathrm{MSC}} \\ M_{\mathrm{q0}}^{\mathrm{MSC}} \end{bmatrix}$. $I_{\mathrm{d0}}^{\mathrm{MSC}}$ and $I_{\mathrm{q0}}^{\mathrm{MSC}}$ are the steady state currents. Consequently, from (A.2)-(A.3), the MSC three ports module i.e. $\left[\boldsymbol{Y}_{\mathrm{dq}}^{\mathrm{MSC}}\right]_{3\times3}$ in Fig. 4 (a) is obtained.

### C. Impedance modeling of the GSC module

Derivation of GSC three ports module is similar to the MSC, by linearizing GSC control blocks, the following equation can be obtained:

$$\begin{bmatrix} i_{\mathrm{d}}^{\mathrm{GSC}} \\ i_{\mathrm{q}}^{\mathrm{GSC}} \end{bmatrix} = \boldsymbol{Y}_{\mathrm{dq}}^{\mathrm{GSC}}\begin{bmatrix} u_{\mathrm{d}}^{\mathrm{GSC}} \\ u_{\mathrm{q}}^{\mathrm{GSC}} \end{bmatrix} + \boldsymbol{a}_{2\times1}^{\mathrm{GSC}} \cdot u_{dc} \tag{A.4}$$

where, $\boldsymbol{Y}_{\mathrm{dq}}^{\mathrm{GSC}} = -\left(\boldsymbol{Z}_{\mathrm{f}}(s) + H_{\mathrm{c}}V_{\mathrm{dc0}}\boldsymbol{I}\right)^{-1}\boldsymbol{G}_{\mathrm{pll}}(s)$;

$\boldsymbol{a}_{2\times1}^{\mathrm{GSC}} = \left(\boldsymbol{Z}_{\mathrm{f}}(s) + H_{\mathrm{c}}V_{\mathrm{dc0}}\boldsymbol{I}\right)^{-1}\begin{bmatrix} H_{\mathrm{c}}H_{\mathrm{dc}}V_{\mathrm{dc0}} + M_{\mathrm{d0}}^{\mathrm{GSC}} \\ M_{\mathrm{q0}}^{\mathrm{GSC}} \end{bmatrix}$;

$T_{\mathrm{pll}}(s) = \frac{U_0 H_{\mathrm{pll}}(s)}{s + U_0 H_{\mathrm{pll}}(s)} \cdot \frac{1}{U_0}$;

$\boldsymbol{Z}_f = \begin{bmatrix} R_{\mathrm{f}} + sL_{\mathrm{f}} & -\omega_{\mathrm{s}}L_{\mathrm{f}} \\ \omega_{\mathrm{s}}L_{\mathrm{f}} & R_{\mathrm{f}} + sL_{\mathrm{f}} \end{bmatrix}$

$\boldsymbol{G}_{\mathrm{pll}}(s) = \begin{bmatrix} 1 & \left(H_{\mathrm{c}}I_{\mathrm{q0}}^{\mathrm{GSC}} + M_{\mathrm{q0}}^{\mathrm{GSC}}\right)\frac{V_{\mathrm{dc0}}T_{\mathrm{pll}}(s)}{U_0} \\ 0 & 1 - \left(H_{\mathrm{c}}I_{\mathrm{d0}}^{\mathrm{GSC}} + M_{\mathrm{d0}}^{\mathrm{GSC}}\right)\frac{V_{\mathrm{dc0}}T_{\mathrm{pll}}(s)}{U_0} \end{bmatrix}$; and $H_{\mathrm{pll}}$ is the PI controller of PLL. Then, according to the principle of power balance between ac and dc side of GSC, yields:

$$i_{dc}^{\mathrm{GSC}} = \boldsymbol{b}_{1\times2}^{\mathrm{GSC}}\begin{bmatrix} u_{d}^{\mathrm{GSC}} \\ u_{q}^{\mathrm{GSC}} \end{bmatrix} + \boldsymbol{Y}_{\mathrm{dc}}^{\mathrm{GSC}} \cdot u_{dc} \tag{A.5}$$

where,

$Y_{\mathrm{dc}}^{\mathrm{GSC}} = \frac{3}{2}\left\{\begin{bmatrix} M_{\mathrm{d0}}^{\mathrm{GSC}} - I_{\mathrm{d0}}^{\mathrm{GSC}}H_{\mathrm{c}} & M_{\mathrm{q0}}^{\mathrm{GSC}} - I_{\mathrm{q0}}^{\mathrm{GSC}}H_{\mathrm{c}} \end{bmatrix}\boldsymbol{a}_{2\times1}^{\mathrm{GSC}}\right\}$, $+I_{\mathrm{d0}}^{\mathrm{GSC}}H_{\mathrm{c}}H_{\mathrm{dc}}$

and,

$\boldsymbol{b}_{1\times2}^{\mathrm{GSC}} = \frac{3}{2}\left\{\begin{bmatrix} M_{\mathrm{d0}}^{\mathrm{GSC}} - I_{\mathrm{d0}}^{\mathrm{GSC}}H_{\mathrm{c}} & M_{\mathrm{q0}}^{\mathrm{GSC}} - I_{\mathrm{q0}}^{\mathrm{GSC}}H_{\mathrm{c}} \end{bmatrix}\cdot\boldsymbol{Y}_{\mathrm{dq}}^{\mathrm{GSC}} - \begin{bmatrix} I_{\mathrm{d0}}^{\mathrm{GSC}}\left(H_{\mathrm{c}}I_{\mathrm{q0}}^{\mathrm{GSC}} + M_{\mathrm{q0}}^{\mathrm{GSC}}\right) \\ -I_{\mathrm{q0}}^{\mathrm{GSC}}\left(H_{\mathrm{c}}I_{\mathrm{d0}}^{\mathrm{GSC}} + M_{\mathrm{d0}}^{\mathrm{GSC}}\right) \end{bmatrix}^{\mathrm{T}}\cdot\frac{T_{\mathrm{pll}}(s)}{U_0}\right\}$.

Consequently, from (A.4)-(A.5), the MSC three ports module i.e. $\left[\boldsymbol{Y}_{\mathrm{dq}}^{\mathrm{GSC}}\right]_{3\times3}$ in Fig. 4 (a) can be assembled.

### D. Impedance modeling of the AC grid module

The grid impedance is:

$$\boldsymbol{Z}_{\mathrm{dq}}^{\mathrm{Grid}} = \begin{bmatrix} R_{\mathrm{g}} + sL_{\mathrm{g}} & -\omega_{\mathrm{s}}L_{\mathrm{g}} \\ \omega_{\mathrm{s}}L_{\mathrm{g}} & R_{\mathrm{g}} + sL_{\mathrm{g}} \end{bmatrix} \tag{A.6}$$

where $R_{\mathrm{g}}$ is the grid resistance and $L_{\mathrm{g}}$ is the inductance, including the step-up transformer's leakage inductance.

### E. Effects of the dc capacitor size on the phase margin

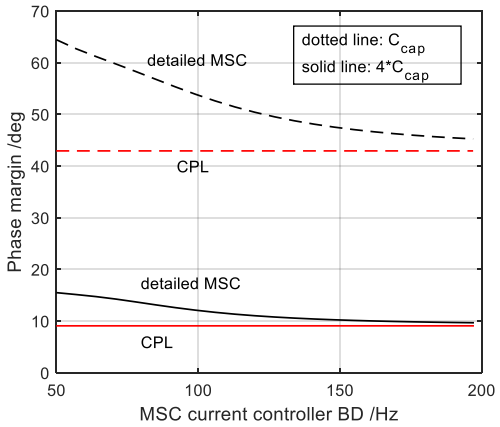


Fig. A1 Effects of the dc capacitor size on the phase margin (PLL = 20 Hz, current controller of GSC is 200 Hz, dc voltage controller is 20 Hz, SCR = 4, $P_0$ = 0.35 p.u.)

As can be seen from Fig. A1, for a regular dc capacitor size, the difference in phase margin between the CPL-based and the detailed model is evident. However, if the capacitor size is increased by 4 times, then the difference becomes small, indicating that the MSC modeling effects can be neglected if the dc capacitor is sufficient large.

However, in engineering, there is always a tendency to minimize the capacitor size to achieve a smaller package for installation. Considering this fact, a large dc capacitor probably is not a good assumption, thus the MSC modeling effects should not be neglected.

## REFERENCES

[1]. R. Teodorescu, M. Liserre, and P. Rodriguez, "Introduction," in Grid converters for photovoltaic and wind power systems, Chichester, United

Kingdom: John Wiley & Sons, 2011, pp. 1–4.
[2]. N. Flourentzou, V. G. Agelidis and G. D. Demetriades, "VSC-Based HVDC Power Transmission Systems: An Overview," in IEEE Transactions on Power Electronics, vol. 24, no. 3, pp. 592-602, March 2009.
[3]. C. Li, "Unstable Operation of Photovoltaic Inverter From Field Experiences," in IEEE Transactions on Power Delivery, vol. 33, no. 2, pp. 1013-1015, April. 2018.
[4]. H. Liu, X.X. Xie, J.B. He, T. Xu, Z. Yu, C. Wang, C.Y. Zhang, "Subsynchronous Interaction Between Direct-Drive PMSG Based Wind Farms and Weak AC Networks," in IEEE Transactions on Power Systems, vol. 32, no. 6, pp. 4708-4720, Nov. 2017.
[5]. L. P. Kunjumuhammed, B. C. Pal, C. Oates and K. J. Dyke, "Electrical Oscillations in Wind Farm Systems: Analysis and Insight Based on Detailed Modeling," in IEEE Transactions on Sustainable Energy, vol. 7, no. 1, pp. 51-62, Jan. 2016.
[6]. J. Sun. "Impedance-Based Stability Criterion for Grid-Connected Inverters," IEEE Trans. Power Electron, vol.26, no. 11, pp. 3075–3078, 2011.
[7]. W. Ren and E. Larsen, "A Refined Frequency Scan Approach to Sub-Synchronous Control Interaction (SSCI) Study of Wind Farms," in IEEE Transactions on Power Systems, vol. 31, no. 5, pp. 3904-3912, Sept. 2016.
[8]. B. Wen, D. Boroyevich, R. Burgos, P. Mattavelli and Z. Shen, "Inverse Nyquist Stability Criterion for Grid-Tied Inverters," in IEEE Transactions on Power Electronics, vol. 32, no. 2, pp. 1548-1556, Feb. 2017.
[9]. J. Sun, "Small-Signal Methods for AC Distributed Power Systems–A Review," in IEEE ESTS., Baltimore, Maryland, pp .44–52, 2009.
[10]. Belkhayat M, "Stability criteria for AC power systems with regulated loads," Ph.D. dissertation, Purdue University, USA, 1997.
[11]. M. Cespedes and J. Sun, "Impedance Modeling and Analysis of Grid-Connected Voltage-Source Converters," in IEEE Transactions on Power Electronics, vol. 29, no. 3, pp. 1254-1261, March 2014.
[12]. B. Wen, D. Boroyevich, R. Burgos, P. Mattavelli and Z. Shen, "Small-Signal Stability Analysis of Three-Phase AC Systems in the Presence of Constant Power Loads Based on Measured d-q Frame Impedances," in IEEE Transactions on Power Electronics, vol. 30, no. 10, pp. 5952-5963, Oct. 2015.
[13]. L. Harnefors, "Modeling of Three-Phase Dynamic Systems Using Complex Transfer Functions and Transfer Matrices," IEEE Trans. Ind. Electron, vol. 54, no. 4, pp. 2239–2248, 2007
[14]. X. Wang, L. Harnefors, F. Blaabjerg, and P.C. Loh, "A Unified Impedance Model of Voltage-Source Converters with Phase-Locked Loop Effect," IEEE ECCE, United States, pp. 1–8, 2016.
[15]. A. Rygg, M. Molinas, C. Zhang and X. Cai, "A Modified Sequence-Domain Impedance Definition and Its Equivalence to the dq-Domain Impedance Definition for the Stability Analysis of AC Power Electronic Systems," in IEEE Journal of Emerging and Selected Topics in Power Electronics, vol. 4, no. 4, pp. 1383-1396, Dec. 2016.
[16]. C. Zhang, X. Cai, A. Rygg and M. Molinas, "Sequence Domain SISO Equivalent Models of a Grid-Tied Voltage Source Converter System for Small-Signal Stability Analysis," in IEEE Transactions on Energy Conversion, vol. 33, no. 2, pp. 741-749, June 2018.
[17]. S. Shah and L. Parsa, "Impedance Modeling of Three-Phase Voltage Source Converters in DQ, Sequence, and Phasor Domains," in IEEE Transactions on Energy Conversion, vol. 32, no. 3, pp. 1139-1150, Sept. 2017.
[18]. M. K. Bakhshizadeh, X. Wang, F. Blaabjerg, J. Hjerrild, L. Kocewiak, C. L. Bak, and B. Hesselbæk, "Couplings in Phase Domain Impedance Modeling of Grid-Connected Converters," IEEE Trans. Power Electron, vol. 31, no. 10, pp. 6792–6796, 2016.
[19]. C. Zhang, X. Cai, Z. Li, A. Rygg, M. Molinas, "Properties and Physical Interpretation of the Dynamic Interactions between Voltage Source Converters and Grid: Electrical Oscillation and Its Stability Control," IET Power Electron, vol. 10, no. 8, pp. 894–902.
[20]. S. Shah, I. Vieto, Nian Heng and J. Sun, "Real-time simulation of wind turbine converter-grid systems," 2014 International Power Electronics Conference, Hiroshima, pp. 843-849, 2014.
[21]. J. Hu, Q. Hu, B. Wang, H. Tang and Y. Chi, "Small Signal Instability of PLL-Synchronized Type-4 Wind Turbines Connected to High-Impedance AC Grid During LVRT," in IEEE Transactions on Energy Conversion, vol. 31, no. 4, pp. 1676-1687, Dec. 2016.
[22]. E. Ebrahimzadeh, F. Blaabjerg, X. Wang and C. L. Bak, "Harmonic Stability and Resonance Analysis in Large PMSG-Based Wind Power Plants," in IEEE Transactions on Sustainable Energy, vol. 9, no. 1, pp. 12-23, Jan. 2018.
[23]. Y. Xu, H. Nian, T. Wang, L. Chen and T. Zheng, "Frequency coupling characteristic modeling and stability analysis of doubly fed induction generator," in IEEE Transactions on Energy Conversion, 2018 (online).
[24]. I. Vieto and J. Sun, "Sequence Impedance Modeling and Analysis of Type-III Wind Turbines," in IEEE Transactions on Energy Conversion, vol. 33, no. 2, pp. 537-545, June 2018.
[25]. L. Xu, L. Fan and Z. Miao, "DC Impedance-Model-Based Resonance Analysis of a VSC–HVDC System," in IEEE Transactions on Power Delivery, vol. 30, no. 3, pp. 1221-1230, June 2015.
[26]. M. Amin, M. Molinas, J. Lyu and X. Cai, "Impact of Power Flow Direction on the Stability of VSC-HVDC Seen From the Impedance Nyquist Plot," in IEEE Transactions on Power Electronics, vol. 32, no. 10, pp. 8204-8217, Oct. 2017.
[27]. C. Desoer and Yung-Terng Wang, "On the generalized nyquist stability criterion," in IEEE Transactions on Automatic Control, vol. 25, no. 2, pp. 187-196, April 1980.
[28]. E. Möllerstedt, "Dynamic analysis of harmonics in electrical systems," Ph.D. dissertation, Lund University, Sweden, 2000.

**Chen Zhang** received the B.Eng. degree in electrical engineering from the China University of Mining and Technology, Xuzhou, China, in 2011, and the Ph.D degree from Shanghai Jiao Tong University (SJTU), shanghai, China, in 2018. He is currently working as a postdoctoral researcher at Norwegian University of Science and Technology (NTNU), Trondheim, Norway. His research interest is the modeling and stability analysis of the power-electronics-based systems, where the aim is to reveal the fundamental mechanisms of stability issues brought about by VSCs.

**Xu Cai** received the B.Eng. degree from Southeast University, Nanjing, China, in 1983, and the M.Sc. and Ph.D. degrees from the China University of Mining and Technology, Xuzhou, China, in 1988 and 2000, respectively. He was with the Department of Electrical Engineering, China University of Mining and Technology, as an Associate Professor from 1989 to 2001. He was the Vice Director of the State Energy Smart Grid R&D Center, Shanghai, China, from 2010 to 2013. He has been with Shanghai Jiao Tong University, Shanghai, as a Professor since 2002, where he has also been the Director of the Wind Power Research Center since 2008. His current research interests include power electronics and renewable energy exploitation and utilization, including wind power converters, wind turbine control system, large power battery storage systems, clustering of wind farms and its control system, and grid integration.

**Marta Molinas** (M'94) received the Diploma degree in electromechanical engineering from the National University of Asuncion, Asuncion, Paraguay, in 1992; the Master of

Engineering degree from Ryukyu University, Japan, in 1997; and the Doctor of Engineering degree from the Tokyo Institute of Technology, Tokyo, Japan, in 2000. She was a Guest Researcher with the University of Padova, Padova, Italy, during 1998. From 2004 to 2007, she was a Postdoctoral Researcher with the Norwegian University of Science and Technology (NTNU) and from 2008-2014 she has been professor at the Department of Electric Power Engineering at the same university. She is currently Professor at the Department of Engineering Cybernetics, NTNU. Her research interests include stability of power electronics systems, harmonics, instantaneous frequency, and non-stationary signals from the human and the machine. She is Associate Editor for the IEEE Journal JESTPE, IEEE PELS Transactions and Editor of the IEEE Transactions on Energy Conversion. Dr. Molinas has been an AdCom Member of the IEEE Power Electronics Society from 2009 to 2011.

**Atle Rygg** received the MSc degree in Electrical Engineering from the Norwegian University of Science and Technology (NTNU) in 2011. From 2011 to 2015 he was a research scientist at SINTEF Energy Research in the field of power electronics. He is currently pursuing his PhD-degree at department of engineering cybernetics at NTNU. His topic or research is impedance based stability analysis of power electronic systems, where the aim is to contribute to the fundamental understanding in this family of methods.